

RIGA TECHNICAL UNIVERSITY

Faculty of Materials Science and Applied Chemistry

Institute of Silicate Materials

Līga Grase

Doctoral Student of the Study Programme “Materials Science”

**PHASE TRANSITIONS IN Sn_xS_y THIN FILMS
AND THEIR PROPERTIES**

Summary of the Doctoral Thesis

Scientific supervisors

Professor Dr. habil. sc. ing.
GUNDARS MEŽINSKIS

Professor Dr. habil. phys.
ARTŪRS MEDVIDS

**RTU Press
Rīga 2017**

Grase L. Phase transitions in Sn_xS_y Thin Films and their Properties. Summary of the Doctoral Thesis. – Riga: RTU Press, 2017. – 29 p.

Printed in accordance with the decision of the Promotion Council “[RTU P-18]” of 29 September, 2017, Minutes No. 9.

DOCTORAL THESIS PROPOSED TO RIGA TECHNICAL UNIVERSITY FOR THE PROMOTION TO THE SCIENTIFIC DEGREE OF DOCTOR OF ENGINEERING SCIENCES

To be granted the scientific degree of Doctor of Engineering Sciences, the present Doctoral Thesis has been submitted for the defence at the open meeting of RTU Promotion Council on December 15, 2017 at the Faculty of Materials Science and Applied Chemistry of Riga Technical University, 3/7 Paula Valdena Street, Room 272.

OFFICIAL REVIEWERS

Professor Dr. habil. phys. Baiba Bērziņa
University of Latvia, Latvia

Professor Dr. phys. Edmunds Tamanis
University of Daugavpils, Latvia

Professor Dr. habil. phys. Steponas Ašmontas
State Research Institute Centre for Physical Sciences and Technology, Lithuania

DECLARATION OF ACADEMIC INTEGRITY

I hereby declare that the Doctoral Thesis submitted for the review to Riga Technical University for the promotion to the scientific degree of Doctor of Engineering Sciences is my own. I confirm that this Doctoral Thesis had not been submitted to any other university for the promotion to a scientific degree.

Līga Grase (signature)

Date:

The Doctoral Thesis has been written in Latvian. It consists of Introduction; 3 chapters; Conclusion; 46 figures; 3 tables; 1 appendix; the total number of pages is 84. The bibliography contains 110 titles.

ACKNOWLEDGMENTS

I would like to express my sincere gratitude to my scientific supervisors Professor Dr. habil. sc. ing. Gundars Mežinskis for the opportunity to work with modern scientific equipment, for advice in the development of the doctoral thesis, opportunity to participate in SEM-FIB-AFM training school (Istanbul, Turkey) and CERN study tour (Geneva, Switzerland), and Professor Dr. habil. phys. Artūrs Medvids for valuable discussions, newly acquired knowledge in laser processing, as well as for the opportunity to participate in international conference Inter-Academa 2015 (Hamamatsu, Japan) and preparation for this conference, which resulted in “The Best Presentation Award for Young Researchers”.

Many thanks to my colleagues Dr. Volodymyr Kosyak and Andrii Voznyi from the Sumi State University (Ukraine) for providing research samples (SnS_2 thin films), participation in research experiments and interpretation of the results, as well as for many valuable discussions.

I would like to thank Professor Dr. Algirdas Selskis for collaboration and opportunity to carry out significant research using FIB-FESEM equipment, as well as for the opportunity to exchange knowledge and experience by working with high resolution scanning electron microscopes.

I would also like to thank the staff members of the Institute of Technical Physics and Institute of Silicate Materials, especially to Dr. phys. Pāvels Onufrijevs for training me to work with Nd:YAG laser equipment, and valuable discussions about laser-matter interactions with different materials, and to Māris Rundāns for valuable discussions related to the substructure of studied material Sn_xS_y . Thanks also to Jana Vecstaudža for XRD measurements.

Finally, I would like to express my thanks to my family for encouragement and support.

CONTENTS

LIST OF ABBREVIATIONS	6
GENERAL OVERVIEW	7
LITERATURE REVIEW	9
EXPERIMENTAL METHODOLOGY	12
1. Preparation of SnS ₂ thin films	12
2. Thermal vacuum annealing of SnS ₂ thin films	12
3. Laser irradiation of SnS ₂ thin films by second harmonic Nd:YAG laser	12
4. Investigation of properties of Sn _x S _y thin films before and after different treatments	12
5. I–V Characteristics	13
RESULTS	14
1. Characterization of properties of obtained SnS ₂ thin films	14
2. SnS ₂ – SnS phase transition by thermal vacuum annealing	15
3. Laser-induced phase transitions in Sn _x S _y	18
The mechanism of laser induced phase transitions in Sn _x S _y thin films	23
I–V characteristics	23
4. Formation of metallic layer of Sn on the surface of SnS ₂ -SnS	24
GENERAL CONCLUSIONS	25
APPROBATION OF WORK	26
REFERENCES	27

LIST OF ABBREVIATIONS

CSS – close spaced sublimation
 T_s – substrate temperature
 T_e – evaporator temperature
 T_w – wall temperature
ITO – indium-doped tin oxide
FESEM – field emission scanning electron microscope
FIB – focused ion beam
AFM – atomic force microscope
XRD – X-ray diffractometer
EDS – energy dispersive X-ray spectroscopy
RS – Raman spectroscopy
IR – infrared radiation
OM – optical microscope
RMS – root mean square
FWHM – full width at half maximum
 λ – wavelength, nm
 α – absorption coefficient, cm^{-1}
I-V – current-voltage
R – peak intensity ratio
Nd:YAG – neodymium doped yttrium aluminium garnet
 τ – pulse duration, ns
COD – crystallography open database
SILAR – successive ionic layer adsorption and reaction
 I – intensity, MW/cm^2
 V_{Sn} – tin vacancies
 V_{S} – sulphur vacancies
 Sn_i – tin interstitials
 S_i – sulphur interstitials
CIGS – $\text{Cu}(\text{In},\text{Ga})\text{Se}_2$
CZTS – $\text{Cu}_2\text{ZnSnS}_4$
 F – force exerted on the impurity atoms in the presence of temperature gradient
 Q^* – heat of transfer for an atom or a vacancy
 x – coordinate directed from the surface to the bulk of a semiconductor
 N – concentration of the impurity atoms
 E_a – activation energy

GENERAL OVERVIEW

Research topicality

Binary compounds Sn_xS_y have high potential use in optoelectronics. In particular, SnS_2 with n-type conductivity is a promising material for photodetectors and for window layers in solar cells (with the potential to replace CdS) due to high carrier mobility and wide band gap of 2.24 eV [1]. Whereas SnS p-type semiconductor exhibits unique properties for application in solar cells as absorber layer instead of the traditional CdTe and CIGS. These properties include the optimal band gap of 1.1 eV [2], [3] and the high optical absorption coefficient [4]. Hence, the theoretical efficiency of SnS solar cells is 24 % [5], [6]. Other important advantages of Sn_xS_y compounds are their low-cost, earth abundance and non-toxicity. Despite these facts, the record efficiency of SnS solar cells is only 4,4 % [7]. Encouraging progress in efficiency of SnS based solar cells was achieved in Massachusetts Institute of Technology [8]. Such low efficiency is explained by non-homogeneity of Sn_xS_y due to the formation of secondary phases and presence of different types of defects.

Two-dimensional structure of Sn_xS_y compounds opens pathway to their use in nanoelectronics. SnS_2 are actively studied as a base layer for fast photo detectors analogously to WS_2 and MoS_2 .

The laser technology could give a new impulse to the development of high performance Sn_xS_y based devices. Laser technology allows accomplishing of specific tasks related to the improvement of material performance, which cannot be solved by conventional approaches, such as thermal annealing and optimization of growth conditions. It is a powerful tool allowing the improvement of the crystal quality of highly disordered polycrystalline films as well as phase transition in compound semiconductors [9]. For Sn_xS_y compounds, the controlling of secondary phase formation is an important task since SnS_2 could be easily transformed to SnS and vice versa by changing of volatile S concentration. On the other hand, the existence of Sn_xS_y phases with different optical and electrical properties opens completely new opportunities to produce thin film heterojunction devices based on the same components of compound.

Laser induced phase transitions are a new direction of research and can be used for the formation of more energy-efficient and cheaper micro/nanoscale structures in microelectronics and optoelectronics, whereas the existing methods, such as molecular beam epitaxy, chemical vapor deposition, etc. are expensive and are realized using complex equipment and technology. In addition, thermal mechanism of laser induced phase transitions, for example, using nanosecond laser radiation, has a significant advantage over the femtosecond laser induced phase transitions, as it does not create high pressure and therefore is not destructive to the structure.

The aim of the Thesis

The aim of the doctoral thesis is to develop a new method for inducing phase transitions in SnS_2 thin films from SnS_2 to SnS and from SnS to Sn by using the second harmonic Nd:YAG laser irradiation, thus obtaining a heterojunction with an electrical contact using one technological process.

Tasks to be carried out

1. To obtain structural investigations of Sn_xS_y thin films, obtained by CSS method, before and after irradiation by laser.
2. To obtain surface morphology and chemical composition investigations of Sn_xS_y thin films, before and after thermal annealing at different annealing temperatures and duration, in order to determine optimal conditions for inducing phase transition from SnS_2 to SnS .
3. SnS_2 thin film surface irradiation by second harmonic Nd:YAG laser to locally induce phase transition in surface layer of SnS_2 thin films to SnS phase in order to form SnS_2/SnS heterojunction.
4. SnS_2 thin film surface irradiation by second harmonic Nd:YAG laser in order to induce phase transition from SnS phase to metallic Sn phase in the surface layer of previously formed heterojunction SnS_2/SnS .

Theses to be defended

1. Phase transition from hexagonal SnS_2 phase to orthorhombic SnS phase is induced by the second harmonic Nd:YAG laser irradiation with laser intensity from 7.0–11.0 MW/cm^2 . In the case of applying laser irradiation intensity from 12.0–15.0 MW/cm^2 , metallic Sn phase is formed on the surface of SnS . By exceeding laser intensity over the intensity threshold $I_{\text{th}} = 15.0 \text{ MW}/\text{cm}^2$, ablation of SnS_2 material takes place.
2. $\text{SnS}_2 \rightarrow \text{SnS}$ and $\text{SnS} \rightarrow \text{Sn}$ phase transition mechanism relates to S atom drift towards the irradiated surface of the sample in the presence of the temperature gradient, followed by S evaporation.

Novelty of the research

For the first time, the possibility of obtaining SnS_2/SnS heterojunction and metallic Sn contact on the surface of SnS by using one technological task using second harmonic Nd:YAG laser irradiation was demonstrated.

Practical significance

The present study is focused on the development and implementation of innovative approach for the production of low-cost optoelectronic devices based on non-toxic earth abundant materials. Successful implementation of the proposed approach will allow replacing the currently used complicated multistage technological process of deposition of multi layers for formation of p-n heterojunction structure by a simple laser irradiation based technique. Also, irradiation-based improvement of crystalline quality will help to fully realize such advantages of Sn_xS_y compounds as high carrier mobility and two-dimensionality.

LITERATURE REVIEW

Experimental practice is often connected with systems of a wide variety of characters, therefore phase and component concepts are used for their description. The phase is a chemically and thermodynamically homogeneous part of the system, which has an interface, separating it from other parts of the system, and which consists of simple parts called components [10]. If the composition of matter corresponds to the same chemical formula but has different thermodynamic characteristics, it is already another phase. It refers also to the same matter in the form of a melt. Depending on the number of phases, one-phase or homogeneous systems and multiphase or heterogeneous structures are distinguished.

Transformations in the phase structure of a system are called phase transitions, and are realized in two cases: 1) if the number of simultaneously arbitrarily varied parameters exceeds the number allowed by the number of thermodynamic degrees of freedom in the system; and 2) if any of system parameters changes in such a wide interval that the phase in question becomes unstable and therefore transforms into another phase [11]. The most important examples of phase transitions are 1) the change of the aggregate state of the matter, which is realized as a transition from an energetically unpreferable phase to an energetically preferable one; 2) various crystalline modifications characterized by the transformation of a matter from one allotropic modification to another; 3) change of electric and magnetic properties of the matter due to phase transitions – ferromagnetic, segnetoelectric, segnetomagnetic, antiferromagnetic and antisegetomagnetic phase transition; as well as 4) phenomena such as superconductivity and superfluidity, which are observed only at low temperatures close to absolute zero [11].

Phase transitions are divided into two broad categories: first-order and second-order phase transitions.

In the phase transition of first order, variation of temperature, pressure or other parameter leads to a jump-like change in such most important primary parameters as density, accumulated amount of internal energy, concentration of components, etc. The most typical examples of the first-order phase transitions are melting and crystallization, evaporation and condensation, sublimation and desublimation [12].

At the second-order phase transition, density and internal energy remain unchanged, therefore, such phase transitions can not be observed with unaided eye. Jump-like changes occur in the derivatives with respect to temperature and pressure: heat capacity, thermal expansion coefficient, various sensitivities, etc. The second-order phase transition occurs in cases where the symmetry of structure of the matter changes (the symmetry may completely disappear or decrease). The second-order phase transition, resulting from the change in symmetry, is described by Landau theory [13].

From the perspective of tin-chalcogenides phase diagram it can be seen that, three intermediate phases – SnS, Sn₂S₃ and SnS₂ are formed in Sn-S system [14]. It should be noted, that SnS and SnS₂ melt congruently, whereas Sn₂S₃ melts peritectically forming a liquid and SnS₂.

From a thermodynamic perspective, the window beneficial for growing and stabilizing single phase SnS₂ films is relatively large [15]. The growth conditions beneficial for growth of SnS films are much more restricted than for SnS₂, therefore to expand the stability window, S/Sn ratio should be equal or little bit above the stoichiometric SnS composition.

Due to the increase of sulphur concentration, stability window narrows and the risk of formation of SnS₂ and Sn₂S₃ phases increases.

SnS₂ has CdI₂-like crystal structure that consists of densely packed atomic layers of tin placed between two layers of sulfur. This compound can exist in the form of several polytypes [16], [17]. The band gap of SnS₂ changes in the range of 2.12–2.14 eV depending on the method of obtaining material and their polytype [4], [18]–[21].

SnS₂ shows contrasting defect properties to SnS [22]. Undoped SnS shows p-type behaviour, whereas SnS₂ shows n type, which are mainly attributed to the tin vacancies and tin interstitials, respectively. The defect features in Sn₂S₃ can be described as a combination of those in SnS and SnS₂, intrinsically Sn₂S₃ showing n-type behaviour. However, the conversion to p-type can be attained by doping with a large monovalent cation, namely, potassium. The ambipolar dopability, coupled with the earth abundance of its constituents, indicates great potential for electronic applications, including photovoltaics.

The properties of tin disulphide compounds are summarized in Table 1.1.

Table 1.1

Properties of Sn_xS_y compounds

Compound	Colour	Concentration		Conductivity type	Crystal lattice structure	Band gap at the room temperature, eV
		S, %	Sn, %			
SnS	Dark gray	50.46	49.54	p	orthorombic	~1.4
SnS ₂	Yellow	68.42	31.58	n	hexagonal	~2.1
Sn ₂ S ₃	Black	60.12	39.88	n	hexagonal	~1.1

Tin disulfide thin films can be obtained using the following methods: ionic layer adsorption and reaction (SILAR) [23], spray pyrolysis [24]–[27], thermal vacuum evaporation [21], [28], plasma-enhanced chemical vapour deposition (PECVD) [29] and dip-coating [30]. Each of the methods of obtaining SnS₂ thin films has its advantages and disadvantages. For example, the spray pyrolysis method allows one to obtain a low-cost thin layer of semiconductor. However, thin film obtained by this method has low crystal quality, which could be improved by post-growth annealing of material in toxic H₂S gas [30], [31]. CSS method is also widely used for obtaining high quality thin films of binary semiconductors [32]–[34], nevertheless for deposition of SnS₂ thin films it was used only in this work [35].

Phase transition mechanism in Sn_xS_y compounds could be explained by the fact that sulphur binding energy is smaller than tin binding energy, therefore due to the evaporation of sulphur atoms phase transition from hexagonal SnS₂ phase to orthorombic SnS phase takes place.

Literature data suggests that different approaches have been used to obtain phase transition from SnS₂ to SnS [36], but in this case it is not possible to obtain heterostructure between SnS₂ and SnS phases.

Irradiation by laser has been rarely used in the processing of Sn_xS_y compounds [37]. At the same time, laser irradiation could be considered as an effective method for controllable phase transition in Sn_xS_y. Irradiation by the pulse laser is a fast and effective way, which could be effectively used for modification of chemical and phase composition of Sn_xS_y thin

films. This opens new possibilities to obtain materials with technological advantages for use in Sn_xS_y -based solar cells and other optoelectronic devices.

Tin sulfides SnS , Sn_2S_3 , and SnS_2 are investigated for a wide variety of applications such as photovoltaics, thermoelectrics, two-dimensional electronic devices, Li ion battery electrodes, and photo-catalysts [22].

The most extensively studied thin film solar cells are based on CuIn(Ga)Se_2 (CIGS) and CdTe as absorber layer materials. CIGS and CdTe are showing high efficiency reached in solar cells (19.2 %, and 16.5 %, respectively), while a serious drawback of mass production of solar cells based on these materials are the problems related to cadmium toxicity and indium scarcity [4]. However, an alternative absorber layer for low cost thin film solar cells technology with competitive properties, such as, low toxicity, abundance, high absorption coefficient ($>10^4 \text{ cm}^{-1}$) and direct band gap laying between 1.3 and 1.5 eV, is semiconductor SnS .

Laser is a device that allows delivering large amount of energy in a confined space. The type of laser interaction is dependent on many factors, such as wavelength, pulse duration, intensity and dose. Laser irradiation induces changes locally in the materials chemical composition, crystal structure and its morphology.

Laser-induced phase transitions [38]–[44] have attracted considerable interest of researchers. Plasma and thermal-induced phase transition mechanisms are known. The first one is valid for ultra-short laser pulses in femtosecond range, the second one – for picosecond and longer laser pulses. In the first case [42]–[44], only the electron system is excited during the laser pulse, and the motion of atoms occurs due to a high pressure, created by laser beam. In the second case, the motion of atoms can occur due to the melting [41], [45] as the lattice is heated or in solid phase without melting [46], [47].

The thermogradient field effect plays major role in redistribution of the impurity atoms and intrinsic point defects [48], as a result, interstitial atoms drift towards the temperature gradient but vacancies – in the opposite direction. The drift of impurity atoms depends on the size of host and impurity atoms.

EXPERIMENTAL METHODOLOGY

1. Preparation of SnS₂ thin films

SnS₂ thin films were obtained in vacuum chamber VUP-5M by CSS method. SnS₂ polycrystalline thin films were deposited on ultrasonic cleaned ITO (300 nm thickness) coated glass substrates. The stoichiometric powder of SnS₂ was used as an initial material for evaporation. The temperature of the evaporator and substrate was 675 °C and 200–450 °C, respectively. The difference in temperature ensured that the SnS₂ vapors were sublimated on the glass substrate. The time of deposition was 4 min. Pressure during deposition was 5×10^{-3} Pa. The distance between the evaporator and the substrate was 1 cm.

CSS method has relatively low costs and allows to produce high-quality semiconductor thin layers under growth conditions close to the thermodynamic equilibrium.

2. Thermal vacuum annealing of SnS₂ thin films

The annealing of the samples was performed in a vacuum oven (10^{-4} Pa) at 300 °C, 400 °C, 500 °C for 30 min, 60 min, 90 min for each temperature and at 600 °C for 30 min. For the convenience, abbreviated names of the samples, which contain corresponding annealing conditions, were used. For instance, S300-30 means that the sample has been annealed at 300 °C for 30 minutes.

3. Laser irradiation of SnS₂ thin films by second harmonic Nd:YAG laser

Laser irradiation of SnS₂ thin films was performed in air by the second harmonic of Nd:YAG laser (Ekspla NL301G irradiation ($\lambda = 532$ nm, $\tau = 4$ ns) in a scanning regime with different number of nanosecond pulses and intensities, which do not exceed material ablation intensity threshold. The samples were irradiated with different laser intensities from 7 MW/cm² to 15 MW/cm². Careful study was performed for laser intensities $I_1 = 8.5$ MW/cm² and $I_2 = 11.5$ MW/cm². The samples were placed on the two-coordinate manipulator, which was controlled by a special computer software, thus allowing to control the speed of movement and movement step. The focused laser beam (spot diameter of 1.5×10^{-3} and 1.3×10^{-3} m for I_1 and I_2 intensities, respectively) was scanned over the sample surface with constant speed of 1.6×10^{-4} m/s and duration of impulse of 4 ns. The scanned area was 0.56×10^{-4} m² for both I_1 and I_2 intensities.

4. Investigation of properties of Sn_xS_y thin films before and after different treatments

The obtained Sn_xS_y samples were characterized before and after different treatments, by using OM, FESEM, FIB/SEM, EDS, AFM, RS and XRD analyses. I–V characteristics were measured after Sn_xS_y samples have been irradiated by laser.

The surface morphology and chemical composition of the thin films were investigated using FEI Nova NanoSEM 650 Schottky field emission scanning electron microscope (FESEM) with an integrated Apollo X energy dispersive spectroscope (EDS). The thickness was measured by FESEM directly from the cross-section of the samples.

Cross-section analysis was also performed with field emission scanning electron microscope Helios NanoLab 650 DualBeam (FEI, The Netherlands) equipped with gallium ion source and platinum deposition system and INCA Energy (Oxford Instruments) EDS.

Room temperature Raman spectroscopy (RS) spectra were studied using Renishaw InVia 90V727 micro-Raman spectrometer. The semiconductor infrared ($\lambda = 785$ nm) and Ar green ($\lambda = 514$ nm) laser were used as an excitation source.

To study the microstructure of the surface and estimate its roughness NT-MDT atomic force microscope (AFM) in a semi-contact mode was used.

Structural analysis was carried out with the help of DRON-4-07 and Rigaku Ultima+ X-ray diffractometers (XRD) using $\text{CuK}\alpha$ radiation source and operating in Bragg-Brentano geometry.

Industrial optical microscope (OM) Nikon ECLIPSE LV150 was used to evaluate Sn_xS_y sample surface morphology.

5. I–V Characteristics

Measurements of the dark current-voltage (I–V) characteristics of ITO/ Sn_xS_y /Al multilayer structures were carried out using Keithley M 6487 pico-amperemeter. In order to avoid formation of Schottky barriers and hence misinterpretation of the results of I–V measurements ohmic Al contacts for the samples were obtained. The Al contacts were deposited by the thermal vacuum evaporation on the surface of as-grown samples and immediately after laser irradiation with different laser intensities at a substrate temperature of 100 °C.

RESULTS

1. Characterization of properties of obtained SnS₂ thin films

Surface and cross-section SEM analysis of single phase SnS₂ thin films, obtained by close space sublimation method, shows that thin films consist of plate-like crystallines, the height of which is similar to the thin film thickness (Fig.1). It was established that the films obtained in the range of the substrate temperature 300 °C to 450 °C are polycrystalline and consist of platelet-shaped grains. The average grain size varies in the range of 0.7–1.2 and depends on substrate temperature T_s. Similar shape of crystallites in SnS₂ thin films were also observed in [49]–[51].

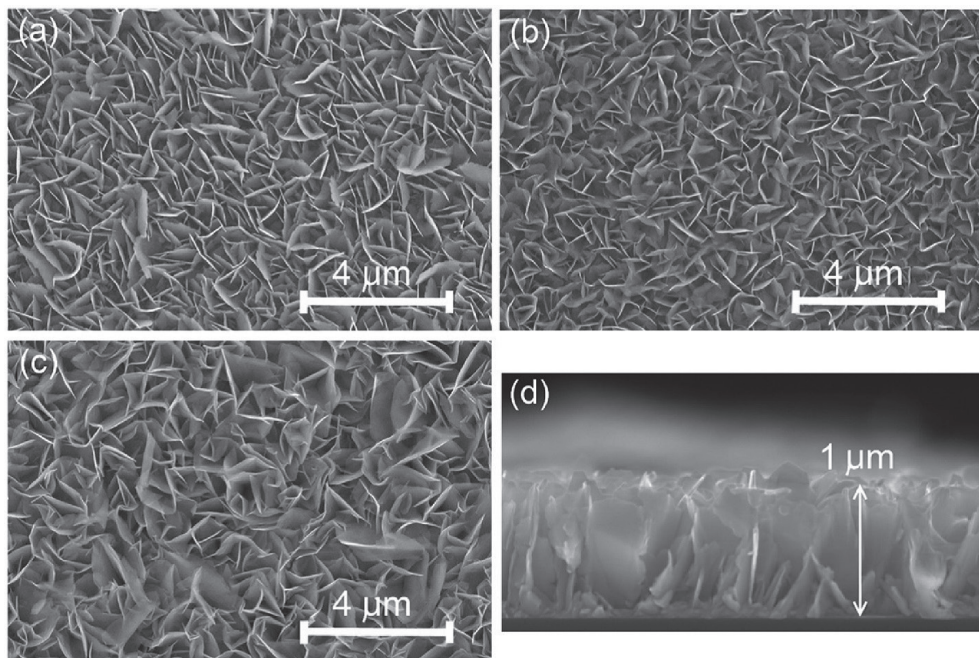


Fig. 1. SEM images of the surface of as-deposited SnS₂ films at (a) 300 °C, (b) 400 °C, and (c) 450 °C, and (d) typical cross-section.

The influence of substrate temperature on the chemical composition of films was studied with EDS. It was established that the composition of all investigated films was close to stoichiometric (35 ± 5 and 65 ± 5 at % for Sn and S, respectively)

The results of AFM study show that the thickness of the platelet-shaped grains decreases from bottom to top in the direction perpendicular to the surface (i.e., perpendicular to the growth front).

From the XRD patterns of the powder and SnS₂ films deposited at different substrate temperatures, it was found that the detected peaks correspond to the hexagonal phase of SnS₂ and orthorhombic phase of Sn₂S₃. Reflections from the crystallographic planes (001), (100), and (002) of the hexagonal phase of SnS₂ had the strongest intensity, while the

intensity of Sn₂S₃-related peaks was very weak. Thus, it could be concluded that the films obtained in the temperature range of 200–450 °C contain mostly hexagonal phase SnS₂ with a small amount (< 3–5 %) of Sn₂S₃ phase.

Raman analysis of SnS₂ thin films confirmed the presence of SnS₂ with a peak at 314.5 cm⁻¹ and a weak peak at 205.6 cm⁻¹. According to theoretical [52] and experimental works [52]–[54], these peaks of SnS₂ are related to A_{1g} and E_g modes, respectively. The FWHM of the peak dominating the A_{1g} mode was no more than 12 cm⁻¹, which indicates a high structural quality of the films. As only the A_{1g} and E_g modes were detected, we can conclude that the obtained films have 2H structure of the SnS₂ polytype [54], [55]. Thus, these results confirm the data of XRD study indicating that the films have a single-phase hexagonal structure.

2. SnS₂ – SnS phase transition by thermal vacuum annealing

Simple approach was demonstrated to obtain single-phase SnS thin films by thermal vacuum annealing of SnS₂ layer obtained by the close-spaced sublimation (CSS) method. It was found that initial non-annealed SnS₂ thin film exhibit typical for SnS₂ chemical composition ratio of Sn/S = 0.49.

EDS measurement reveals that the Sn/S concentration ratio (δ) of the non-annealed SnS₂ film is 0.49 (Fig. 2(a), inset). This value is in good correlation with the reference stoichiometric composition of SnS₂ [14]. It was found that δ value for sample S400-90 is 0.63, which indicates the decreasing of sulphur concentration towards Sn-rich material (Sn₂S₃ and SnS) due to its evaporation. Nearly stoichiometric chemical composition for SnS material [14] of $\delta=0.96$ was obtained for samples S500-30, S500-60 and S500-90 (Fig. 2(d), inset). These results indicate that a post-growth treatment of SnS₂ films at 500 °C leads to the thermal-induced SnS₂-SnS phase transition.

It was shown that the concentration of S gradually decreases with increasing annealing temperature and time. It was found that annealing of the samples at 500 °C for 90 min. provides phase transition from hexagonal SnS₂ to orthorhombic SnS. As it is shown in Fig.3, the shape and the size of platelet-like crystallites were not changed after thermally induced phase transition from SnS₂ → SnS, however, the nano-porous structure was formed.

Annealing of the samples at temperatures below 400 °C (S300-30, S300-60 and S300-90) does not lead to any changes in XRD patterns comparatively with the non-annealed SnS₂ sample. While, the XRD pattern of sample S400-90 shows intensive reflections from (220), (111), (121), (221) planes of orthorhombic Sn₂S₃ phase [56] and (211), (160) planes of orthorhombic SnS phase [57].

The XRD study of the sample S500-30 revealed a significant change in phase composition after annealing. Namely, the SnS-related lines were observed. Only one reflection from (001) plane of SnS₂ phase on XRD spectrum was detected. Thus, a thermal-induced phase transition from hexagonal SnS₂ to orthorhombic SnS takes place. Further increasing of annealing time to 60 min (S500-60) leads to declining in the intensity of (001) SnS₂-related line. Finally, sample S500-90 shows pure SnS phase without traces of SnS₂-related (001) line. It is also worth noting that high intensity of SnS-related lines with low background in XRD pattern indicates high crystal quality of tin monosulphide films.

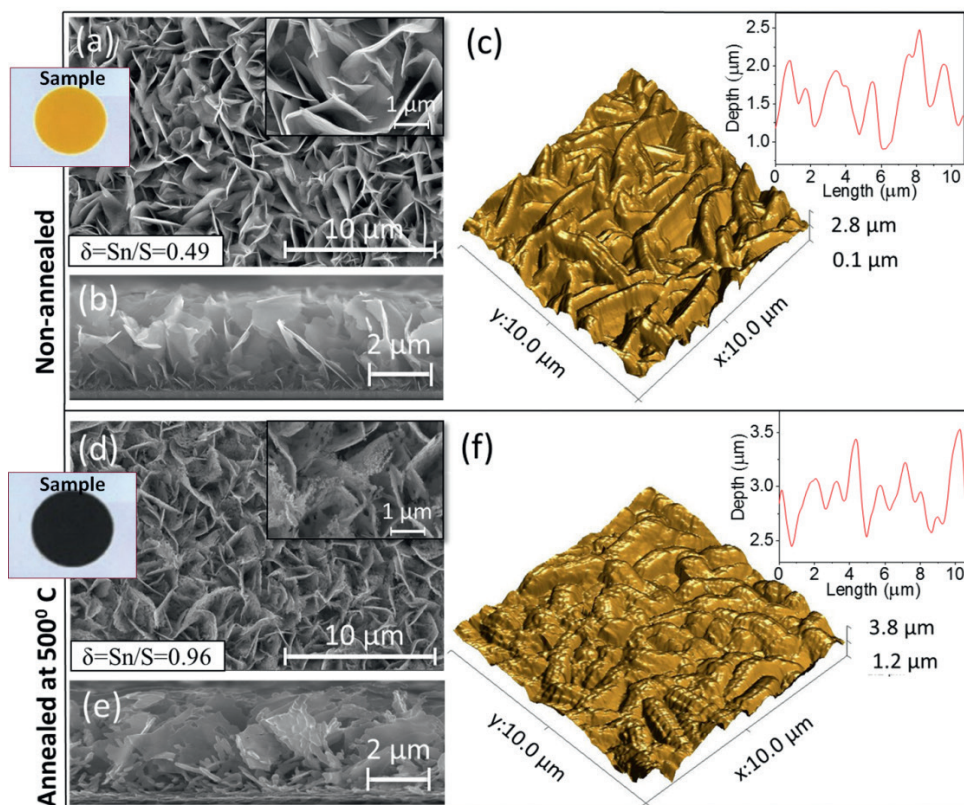


Fig. 2. Surface and cross-sectional morphology of the samples: (a) non-annealed sample – FESEM image of the surface and (b) cross-section; (c) 3D AFM topography with its profile; (d) sample S500-90 – FESEM image of the surface, and (e) cross-section; (f) 3D AFM topography with its profile. The chemical composition ($\delta = \text{Sn}/\text{S}$) measured by EDS are presented in insets.

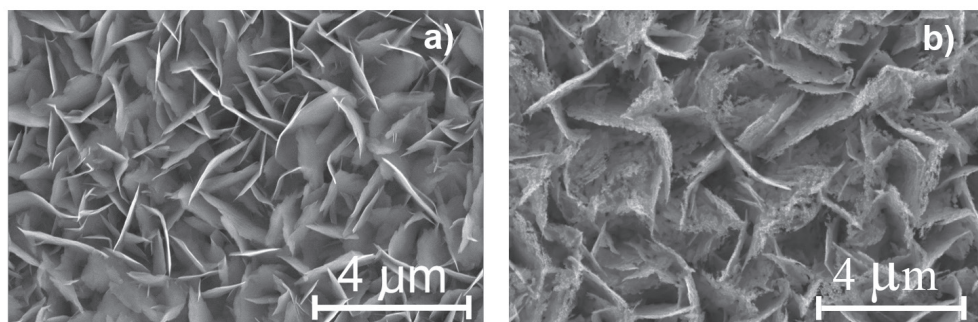


Fig. 3. SnS_2 surface FESEM images: a) before thermal treatment, b) after thermal treatment at 500 °C, 90 min.

The Raman spectra of as-deposited and annealed at different temperatures samples are presented in Fig. 4. As could be seen from Fig. 4(a) the Raman spectrum of the non-annealed sample shows a weak peak around 205 cm^{-1} and a strong peak at 314.5 cm^{-1} which could be assigned to E_g and A_{1g} optical vibration modes of 2H-SnS₂ polytype, respectively [55]. The RS study does not reveal presence of any traces of Sn₂S₃ or SnS phases in samples S300-30 and S300-60, while the Raman spectrum of sample S300-90 (Fig. 4(b)) shows one additional weak peak at 96.5 cm^{-1} . According to the reference data [53], this peak corresponds to A_g mode of SnS compound. It should be noted that XRD analysis shows no secondary phases for the same sample. It can be explained by the small amount of SnS phase in the film. Increasing of annealing temperature to 400 °C (S400-90) leads to increasing in relative intensity of A_g mode of SnS (Fig. 4(c)). The presence of other strong peaks at 285 cm^{-1} and 225 cm^{-1} related to the A_g mode of SnS and a weak peak at 154 cm^{-1} of Sn₂S₃-related A_g mode in this sample were also found [58]. However, the strong mode of SnS₂ at 314.5 cm^{-1} was still observed. It indicates formation of a mixture of SnS, SnS₂ and Sn₂S₃ phases in sample S400-90.

The Raman spectrum of the samples S500-30, S500-60 and S500-90 showed only peaks of SnS-related modes. Namely, the peaks of A_g mode at 95, 193 and 220 cm^{-1} as well as SnS-related B_{2g} mode at 164 cm^{-1} were detected (Fig. 4 (d)). At the same time, XRD analysis

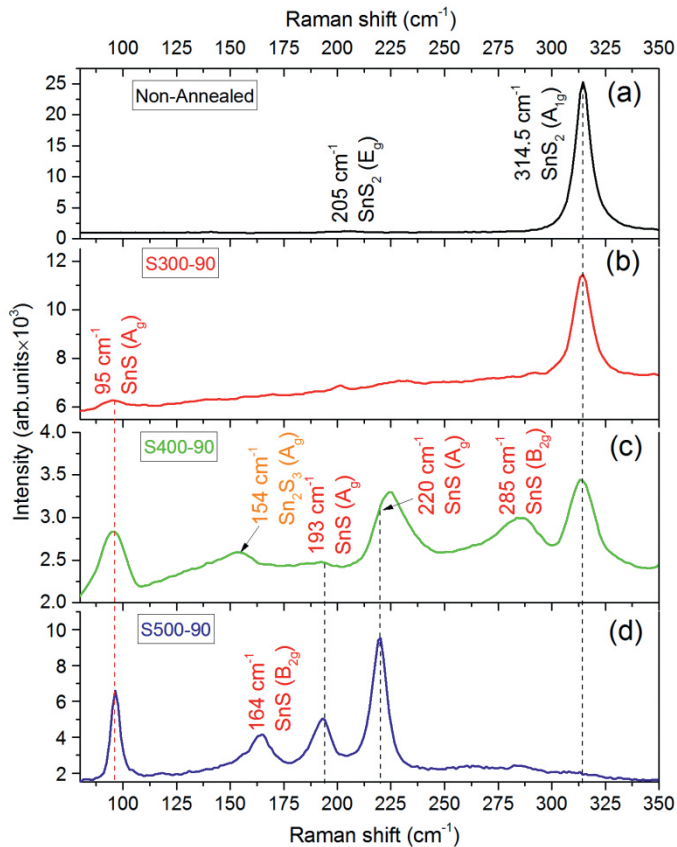


Fig. 4. Raman spectra of samples: (a) non-annealed sample; (b) S300-90 min.; (c) S400-90 min.; and (d) S500-90.

of samples S500-30 and S500-60 revealed traces of SnS₂ phase. Considering the fact that absorption of SnS phase for infrared Raman laser ($\lambda = 785$) is around 200 nm we can conclude that tin disulphide phase is located near the substrate where less intensive sulfur evaporation takes place. Thus, RS study confirms the results of XRD analysis showing that the sample S500-90 is a single-phase SnS.

3. Laser-induced phase transitions in Sn_xS_y

The colour change of samples after irradiation was visually observed. Namely, the colour of the surface of the non-irradiated sample irradiated with I_1 intensity changed from yellow, typical for SnS₂ [4], to dark gray SnS-like colour, which is the evidence of sulfur evaporation and phase transition from SnS₂ to SnS. The colour of the surface of the same regime of irradiation irradiated with intensity I_2 changed to gray. However, the colour of the irradiated surface was lighter.

The FESEM image of the surface of the non-irradiated SnS₂ film (before irradiation) is shown in Fig. 5(a). As can be seen, the thin films consist of plate-like crystallites randomly oriented in a plane parallel to the surface. Higher magnification FESEM image (Fig. 5(a), insert) shows that the length of crystallites is about 1 μm and their thickness is less than 100 nm. It should be noted that the surface of thin film is homogeneous, i.e. free of any large-scale defects and precipitates. The plate-like structure of crystallites is clearly visible on FESEM cross-sectional image presented in Fig. 5(b). Also, it could be seen that the crystallites are well oriented along the plane perpendicular to the surface, in contrast to random growth orientation in the plane parallel to the surface. Such growth orientation is preferable for thin film solar cells. The orientation of crystallites coincided with the direction of current flow and hence less recombination of free carriers on the grain boundaries could be expected. The thickness of the films is about 4.1 μm .

The irradiation of surface with the 8.5 MW/cm² intensity leads to agglomeration and coalescence of grains and formation of islands with 1 μm length (Fig. 5(c)). As could be seen from Fig. 5(c), insert), the surface of the islands is rather homogeneous and does not contain any defects, such as cracks, holes or voids. It should be noted that the image of cross-section FESEM (Fig. 5(d)) clearly shows that the surface after laser irradiation is smoothed and the shape of crystallites has become more roundish. Also, the thickness of the samples has decreased to 3.6 μm due to evaporation of material.

Application of more intensive laser irradiation of 11.5 MW/cm² leads to further enlargement of islands due to agglomeration, and the distance between islands increases. As follows from Fig. 5(e) the average length of islands varies from 1 μm , in this case they have a circular shape (Fig. 5(e), inset), to 5 μm for oblong islands. The cross-section view (Fig. 5(f)) shows that crystallites coalesced to form drop-like islands with an average height of 2.8 μm .

The EDS analysis of the sample irradiated with the intensity of 8.5 MW/cm² (dark gray surface) confirms our assumption that the change in colour from initial yellow to dark gray is due to evaporation of sulphur from the surface. Namely, the surface composition of the irradiated sample is $\delta = 0.72$ (Fig. 5(c)). The EDS analysis of the cross-section (Fig. 5(d)) shows that thickness of the layer with composition $\delta = 0.72$ is about 1 μm . The chemical composition directly next to this layer was $\delta = 0.61$ which is more Sn-rich

than the composition of the nonirradiated sample at the same depth. While chemical composition in the middle of sample cross-section and at the substrate is similar to those in the nonirradiated sample. This reflects that depth of the impact of laser irradiation with the intensity of 8.5 MW/cm^2 is about $2 \mu\text{m}$.

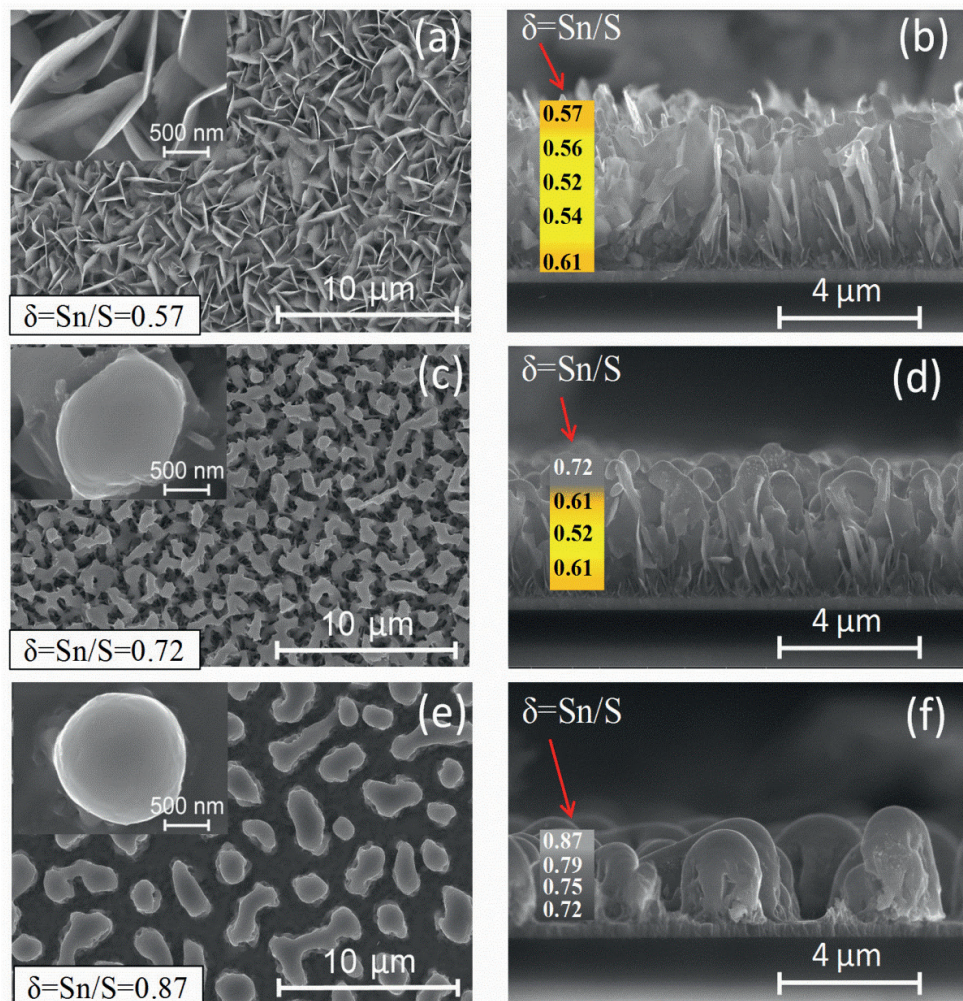


Fig. 5. FESEM images of surface and cross-section of the samples. Non-irradiated sample: (a) surface, (b) cross-section; sample annealed with laser intensity of 8.5 MW/cm^2 : (c) surface, (d) cross-section; sample annealed with laser intensity of 11.5 MW/cm^2 : (e) surface, (f) cross-section. Results of EDS study of chemical composition ($\delta = \text{Sn/S}$) for the surface are presented in insets, and for the cross-section in rectangles (position of δ values in images of cross-section correspond to the spot of measurement).

EDS analysis of the surface irradiated with the intensity of 11.5 MW/cm^2 (light gray surface) shows that the increasing of laser intensity leads to more intensive evaporation of sulfur and hence enrichment of the surface with metal. Namely, the surface chemical

composition was found to be $\delta = 0.87$ (Fig. 5(e)). Also, as follows from Fig. 5(f) the sulphur loss is taking place throughout the depth of the sample. In particular, the concentration of Sn monotonically decreases with depth increasing from $\delta = 0.87$ on the surface to $\delta = 0.72$ at the substrate. Thus, due to the decreased influence of laser irradiation with depth the gradient in Sn concentration was formed.

FIB-SEM images (Fig. 6) show the cross-section of obtained samples, which were obtained by focused ion beam.

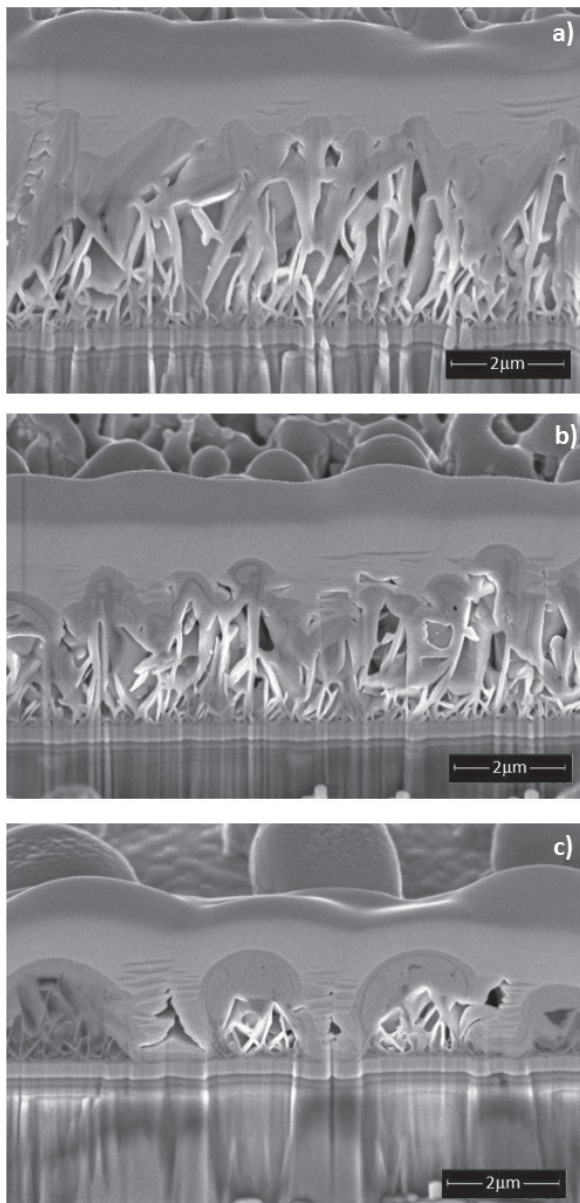


Fig. 6. FIB-SEM cross-section images of SnS₂ thin films a) before and after irradiation with different Nd:YAG laser intensities: b) 8.5 MW/cm²; and c) 11.5 MW/cm².

After irradiation with second harmonic Nd:YAG laser, significant changes in the structure of SnS₂ thin films were observed, namely, irradiation with laser intensity of 8.5 MW/cm² led to interaction volume of about 1 μm, while, the increase of laser radiation intensity up to 11.5 MW/cm² led to changes in chemical composition throughout the whole thin film forming island-like formations consisting of double layered structure.

The irradiation of the sample with the intensity of 8.5 MW/cm² strongly affected the texture of films. As could be seen from XRD pattern the absolute and relative intensity (with respect to the (100) and (101) lines) of the (001) line is significantly decreased while the intensities of line (100) and (101) are increased. This indicates that the bounds along c-direction due to the long-distance van der Waals force are broken and the lattice is compressed. We speculate that this effect could lead to increasing in conductivity of irradiated thin film since the mobility along c-direction is much smaller than along a-direction [57]. In addition to the reorientation of crystal lattice the formation of new phases in irradiated samples were observed. Namely, the (111) SnS-related line at 31.80 becomes clearly visible. Also, weak peaks at 16.20 and 26.60, which correspond to the reflections from (120) and (111), respectively of Sn₂S₃ phase, were detected. Considering the results of EDS analysis of cross-section of the irradiated sample it could be concluded that SnS and Sn₂S₃ phases are mostly located at the surface layer.

For the sample irradiated with the intensity of 11.5 MW/cm² the high (100) and (101) texture of SnS₂ phase remains the same. However, the increasing intensity of (111) SnS-related line as well as (120) and (111) Sn₂S₃-related lines indicates increasing of concentration of these phases. Moreover, the highest intensity of the SnS-related (111) line at 31.80 shows that SnS phase is dominant over SnS₂ and Sn₂S₃ phases.

For the reliable Raman phase analysis of Sn_xS_y compounds the energy of excitation should be close to the band gap of the studied phase. In this case, one can expect high absorption of excitation radiation or even resonance conditions [59] and hence high signal to noise ratio of the Raman spectra. Taking into account the difference between the band gap energies of SnS₂, Sn₂S₃ and SnS compounds we used two wavelengths of excitation. Namely, for identification of SnS₂ phase the excitation with 514 nm green laser is optimal, since the energy of excitation ($E = 2.41$ eV) is close to the band gap of SnS₂ $E_g = 2.24$ eV. While for the identification of Sn₂S₃ and SnS phases with the band gaps of ($E_g = 1.09$ eV) and $E_g = 1.35$ eV the 785 nm IR excitation ($E = 1.58$ eV) is more suitable.

As could be seen from Fig. 7(b), the irradiation of the samples with I_1 intensity leads to the appearance of additional three broad weak peaks centered at 92, 186 and 227 cm⁻¹. Considering the results of EDS and XRD study for the irradiated sample we assumed that these peaks are related to SnS and SnS₂ phases. According to the selection rules [56] the presence and frequencies of Raman modes depend on the orientation of crystal lattice in respect of the direction of the incident and scattered photons. As it was shown in [58] and [56], for most cases the A_g mode related to bonding in the a-c plane is dominant for both SnS and Sn₂S₃ phases. As could be seen from Fig. 7(c) the peak at 92 cm⁻¹ consists of two overlapping peaks at 88 cm⁻¹ and 95 cm⁻¹ related to A_g mode of Sn₂S₃ and SnS phases respectively. The broad weak peak at 189 cm⁻¹ also could be assigned to A_g mode of SnS phase. We speculate that another broad weak peak centred at 227 cm⁻¹ related to two close A_g modes of SnS and Sn₂S₃ at around 220 and 236 cm⁻¹ correspondently. But it is difficult to distinguish the exact position of the peaks. It should be noted that 310 cm⁻¹ Sn₂S₃ was

not observed on the spectrum, probably due to overlapping with the broad A_{1g} mode of SnS_2 phase at 314.7 cm^{-1} .

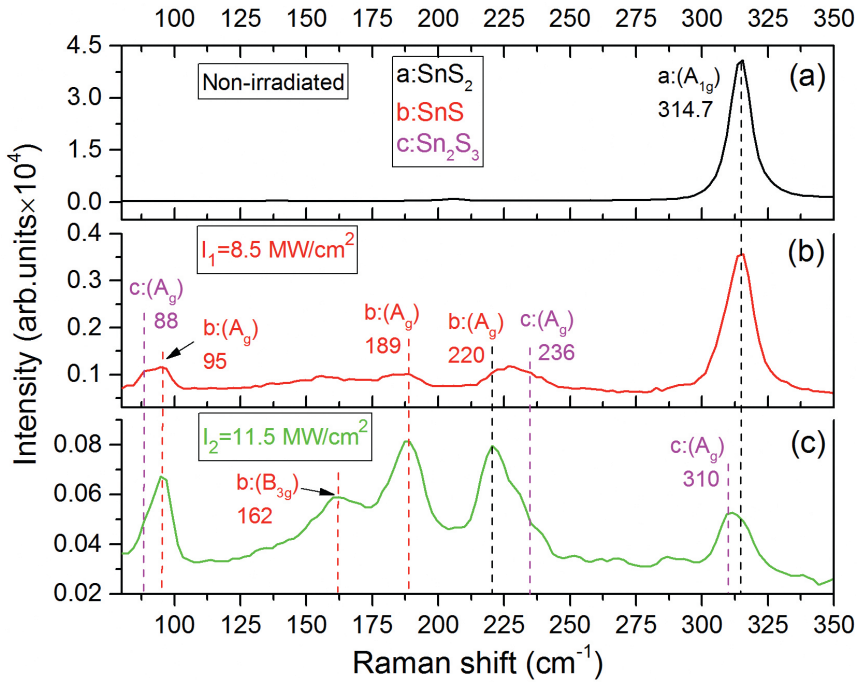


Fig. 7. Raman spectra of the samples obtained with excitation by the green Ar laser $\lambda = 514\text{ nm}$: (a) non-irradiated sample; (b) samples annealed with a laser of 8.5 MW/cm^2 and (c) 11.5 MW/cm^2 intensities.

As was shown in XRD and EDS analysis, the irradiation of the sample with higher intensity of 11.5 MW/cm^2 results in increasing of concentration of SnS and Sn_2S_3 phases. This finding was confirmed by Raman spectroscopy. Namely, the relative intensity of the SnS and Sn_2S_3 -related modes are significantly increased, while the intensity of A_{1g} mode of SnS_2 phase is decreased Fig. 7(c). At that, the SnS -related A_g mode is dominant. Moreover, one more SnS -related B_{3g} mode at 162 cm^{-1} was observed.

In contrast of Raman spectra measured with green excitation, the spectra obtained with IR excitation show strong SnS and Sn_2S_3 -related modes even for the sample irradiated with I_1 intensity. Moreover, the SnS -related A_g mode at 221 cm^{-1} is dominant on both spectra of samples irradiated with I_1 and I_2 intensities. As discussed above, it could be explained by the fact that relatively narrow band gap SnS and Sn_2S_3 compounds interact much stronger with IR than green wavelength radiation. As a result, three peaks of SnS -related A_g mode at 95 cm^{-1} , 187 cm^{-1} and 221 cm^{-1} and peak which could be assigned to the B_{2g} mode at 288 cm^{-1} as well as three peaks of Sn_2S_3 -related A_g mode at 88 cm^{-1} , 154 cm^{-1} and 309 cm^{-1} are clearly observed.

The mechanism of laser induced phase transitions in Sn_xS_y thin films

The mechanism of laser induced phase transition from SnS_2 to SnS is characterized by the formation of heterostructures, such as SnS_2/SnS , due to generation of S interstitials, which has lower defect formation energy $V_s = 1.80$ eV than Sn $V_{\text{Sn}} = 3.16$ eV [4], and its drift towards the irradiated surface of the sample in the gradient of temperature field, the so-called thermogradient effect (TGE) [48]. When the interstitials reach the surface, the intensive evaporation of S atoms takes place. When the ration of Sn/S is close to the stoichiometric content of 50:50, the first order phase transition of hexagonal SnS_2 to ortorombic SnS takes place. A similar mechanism of laser induced phase transition of SnS to Sn is proposed.

I–V characteristics

The I–V curves measured for non-irradiated SnS_2 and irradiated with the intensities of I_1 and I_2 samples are shown in Fig. 8. As can be seen, the I–V curve of ITO/ SnS_2 /Al sample is linear (ohmic). This means that there are no electrical barriers between SnS_2 and Al, or ITO contacts.

The I–V curve of the sample irradiated with the intensity of I_1 shows typical diode behaviour. Alternately, for the I–V curve of the sample irradiated with the intensity of I_2 , the current rectification was much less pronounced.

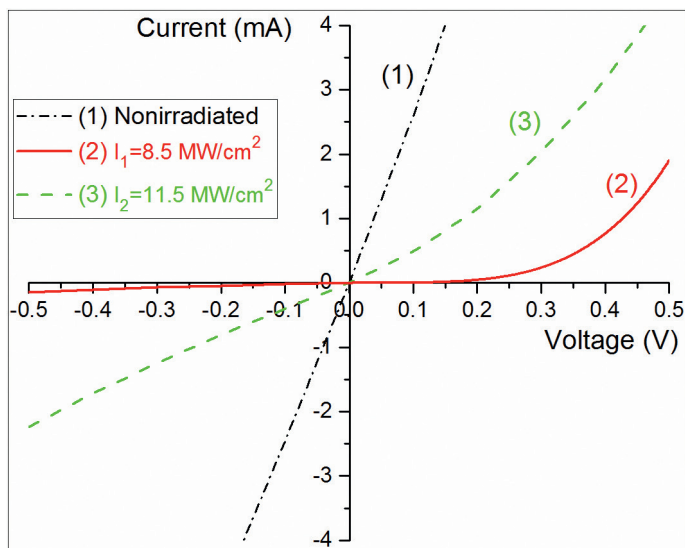


Fig. 8. The current-voltage dependencies of ITO/ Sn_xS_y /Al samples: (1) nonirradiated; (2) samples irradiated with a laser of 8.5 MW/cm^2 and (3) 11.5 MW/cm^2 intensities

Taking into account the results of EDS analysis of the samples cross-section, it could be concluded that in the case of laser irradiation with I_1 intensity a two-layer n- SnS_2 /p- SnS junction was formed which is reflected in diode behaviour of I–V curve.

4. Formation of metallic layer of Sn on the surface of SnS₂-SnS

By increasing laser intensity from 12 MW/cm² to 15 MW/cm² on the surface of previously formed SnS₂-SnS heterostructure (Fig. 9(a)) a metallic Sn contact is formed (Fig. 9(b)). A phase transition from SnS to Sn metallic phase is induced, which is cannot be detected using Raman spectroscopy method. Therefore, Raman spectrum band was not detected, which shows that Sn metallic phase is formed on the surface layer.

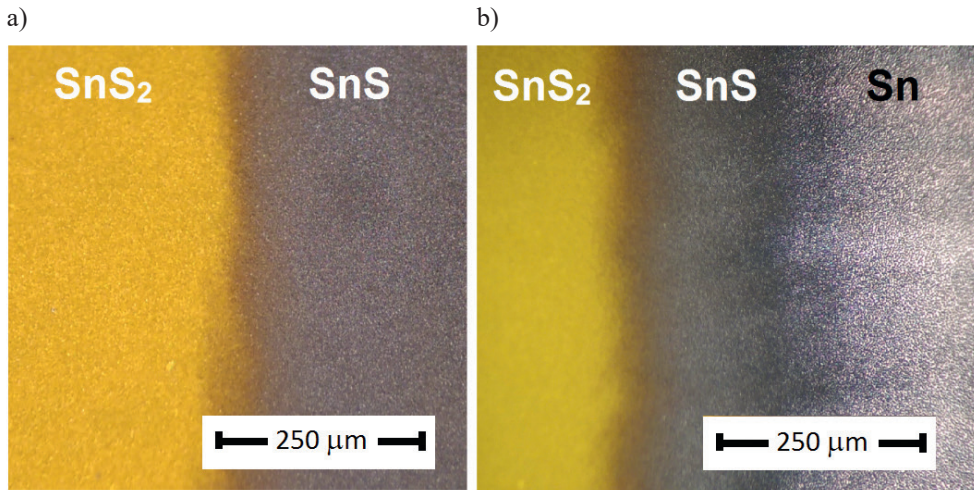


Fig. 9. Optical microscopy images of the sample surface showing phase transition from SnS₂ to SnS and Sn.

The presence of metallic Sn phase on the surface of the sample was confirmed by resistivity measurements, which were carried out by using digital multimeter (Model: GDM-8135) with the smallest scale value of 0.1 Ω. It was found that the sample resistance tends to zero.

GENERAL CONCLUSIONS

1. The results of FESEM, XRD, Raman spectroscopy and EDS analysis confirm, that CSS method is suitable for the deposition of high crystal quality, stoichiometric, single-phase and homogeneous SnS₂ thin films and these thin films have a hexagonal structure of 2H-SnS₂ polytype.
2. The thermal vacuum annealing of the initial SnS₂ thin films at 500 °C (S500-30, S500-60 and S500-90) leads to the decreasing of sulphur concentration and hence provides thermal-induced phase transition from hexagonal SnS₂ to orthorhombic SnS. The shorter time and lower temperature of annealing leads to the mixed phase composition of SnS, Sn₂S₃ and SnS₂. Sample S500-90 exhibits a single-phase orthorhombic Herzenbergite crystal structure with typical for SnS material composition ratio of 0.96. FESEM images showed that the shape and the size of platelet-like crystallites had not changed after thermal annealing, however, significant changes were observed in the microstructure of plate-like crystallines, as the nano-porous structure was formed.
3. For the first time, using the second harmonic of pulsed Nd:YAG laser radiation, the phase transition in SnS₂ polycrystalline thin films from the SnS₂ phase to the SnS phase was induced. This process occurs if the laser radiation intensity is 7 MW/cm² and does not exceed 11 MW/cm². In turn, the intensity of Nd:YAG laser radiation from 12 MW/cm² induces the formation of a metallic Sn-layer on the thin layer of SnS that can be used as an electrical contact in solar cells. When the laser radiation intensity exceeds 15 MW/cm², the Sn_xS_y material ablation takes place. Thus, it is shown that by a single technological process, using the second harmonic of Nd:YAG laser radiation, it is possible to create a n-SnS₂/p-SnS heterostructure with a metallic Sn-layer. I–V characteristics show diodic behaviour, which proves the formation of heterostructure n-SnS₂/p-SnS.
4. The mechanism of laser-induced phase transitions in SnS₂ thin films from SnS₂ to SnS and SnS to Sn is shown. It is explained by the drift of S atoms towards the surface of the sample under the influence of the field of temperature gradient followed by evaporation of subsequent sulfur atoms from the surface.
5. The depth phase distribution in irradiated samples is strongly dependent on the intensity of laser radiation. In particular, the irradiation of the samples with the intensity of $I_1 = 8.5 \text{ MW/cm}^2$ leads to the formation of the SnS layer at the surface. The application of a more intensive irradiation with the intensity of $I_2 = 11.5 \text{ MW/cm}^2$ leads to changes in chemical composition of the whole thin film.

APPROBATION OF WORK

Scientific achievements and main results of the doctoral thesis have been presented at three international conferences, two SCI publications have been published and one patent of the Republic of Latvia has been received.

List of the publications

1. Voznyi, A., Kosyak, V., Opanasyuk, A., Tirkusova, N., **Grase, L.**, Medvids, A., Mezinskis, G. Structural and electrical properties of SnS₂ thin films. Materials Chemistry and Physics, 2016, Vol. 173, pp. 52–61, Article in Press, Available: doi:10.1016/j.matchemphys.2016.01.036 (SCOPUS);
2. Voznyi, A., Kosyak, V., Onufrijevs, P., **Grase, L.**, Vecstaudza, J., Opanasyuk, A., Medvid, A. Laser-induced SnS₂-SnS phase transition and surface modification in SnS₂ thin films. Journal of Alloys and Compounds, 2016, Vol. 688, 130–139. (SCOPUS);
3. Voznyi, A., Kosyak, V., **Grase, L.**, Vecstaudza, J., Onufrijevs, P., Opanasyuk, A., Medvid, A. Formation of SnS phase obtained by thermal vacuum annealing of SnS₂ thin films and its application in solar cells. Materials Science in Semiconductor Processing (*submitted*) (SCOPUS).

Patent of the Republic of Latvia

LV15214 “Fāžu pāreju ierosināšanas paņēmieni alvas sulfīdos”. **L. Grase**, A. Medvids, P. Onufrijevs.

Participation in international conferences

1. Onufrijevs, P., Vozny, A., Kosyak, V., Opanasyuk, A., Medvids, A., **Grase, L.**, Mezinskis, G. Phase Transition in Sn-S based Compounds by Pulsed Laser Radiation. Inter-Academia 2015: The 14th International Conference on Global Research and Education, Japan, Hamamatsu, September 28–30, 2015.
2. **Grase, L.**, Voznyi, A., Kosyak, V., Medvids, A., Mezinskis, G. Structural Properties and Chemical Composition of SnS₂ Thin Films. No: Abstracts of the Riga Technical University 56th International Scientific Conference, Latvia, Riga, October 14–16, 2015. Riga: 2015, p. 27.
3. **Grase, L.**, Voznyi, A., Kosyak, V., Opanasyuk, A., Medvids, A., Onufrijevs, P., Mezinskis, G. Phase Transitions in Sn_xS_y thin films induced by Nd:YAG pulsed laser radiation. BaltSilica 2016: The 7th International Conference on Silicate Materials, Lithuania, Kaunas, May 26–27, 2016.

REFERENCES

- [1] A. Sánchez-Juárez, A. Tiburcio-Silver, and A. Ortiz, "Fabrication of SnS₂/SnS heterojunction thin film diodes by plasma-enhanced chemical vapor deposition," *Thin Solid Films*, Vol. 480–481, pp. 452–456, Jun. 2005.
- [2] J. Vidal, S. Lany, M. D’Avezac, A. Zunger, A. Zakutayev, J. Francis, and J. Tate, "Band-structure, optical properties, and defect physics of the photovoltaic semiconductor SnS," *Appl. Phys. Lett.*, Vol. 100, No. 3, 2012.
- [3] F.-Y. Ran, Z. Xiao, Y. Toda, H. Hiramatsu, H. Hosono, and T. Kamiya, "n-type conversion of SnS by isovalent ion substitution: Geometrical doping as a new doping route.," *Sci. Rep.*, Vol. 5, No. April, p. 10428, 2015.
- [4] L. A. Burton, D. Colombara, R. D. Abellon, F. C. Grozema, L. M. Peter, T. J. Savenije, G. Dennler, and A. Walsh, "Synthesis, Characterization, and Electronic Structure of Single-Crystal SnS, Sn₂S₃, and SnS₂," *Chem. Mater.*, Vol. 25, No. 24, pp. 4908–4916, 2013.
- [5] A. Schneikart, H.-J. Schimper, A. Klein, and W. Jaegermann, "Efficiency limitations of thermally evaporated thin-film SnS solar cells," *J. Phys. D. Appl. Phys.*, Vol. 46, No. 30, p. 305109, 2013.
- [6] J. J. Loferski, "Theoretical considerations governing the choice of the optimum semiconductor for photovoltaic solar energy conversion," *J. Appl. Phys.*, Vol. 27, No. 7, pp. 777–784, 1956.
- [7] P. Sinsersuksakul, L. Sun, S. W. Lee, H. H. Park, S. B. Kim, C. Yang, and R. G. Gordon, "Overcoming Efficiency Limitations of SnS-Based Solar Cells," *Adv. Energy Mater.*, Vol. 4, No. 15, p. n/a-n/a, Oct. 2014.
- [8] V. Steinmann, R. Jaramillo, K. Hartman, R. Chakraborty, R. E. Brandt, J. R. Poindexter, Y. S. Lee, L. Sun, A. Polizzotti, H. H. Park, R. G. Gordon, and T. Buonassisi, "3.88% Efficient Tin Sulfide Solar Cells Using Congruent Thermal Evaporation," *Adv. Mater.*, Vol. 26, No. 44, pp. 7488–7492, 2014.
- [9] S. P. Zhvavyi and G. L. Zykov, "Dynamics of melting and crystallization processes in DdTe under laser irradiation," *Inorg. Mater.*, Vol. 42, No. 7, pp. 717–722, 2006.
- [10] I. Šperberga, U. Sedmalis, G. Sedmale, *Silikatu un gruti kustosū nemetalisku materialu fizikala kimija*. Rīga: RTU Izdevniecība, 2010.
- [11] B. Rolovs, *Termodinamika un statistiskā fizika*. Rīga: Zvaigzne, 1967.
- [12] Базаров И.П., *Термодинамика*. М.: Высшая школа, 1991.
- [13] L. D. Landau, "On the theory of phase transitions," *Zh. Eks. Teor. Fiz.*, Vol. 7, No. 1937, pp. 19–32, 1937.
- [14] R. C. Sharma and Y. A. Chang, "The S-Sn (Sulfur-Tin) System," *J. Phase Equilibria*, Vol. 7, No. 3, pp. 269–273, 1986.
- [15] G. Lindwall, S. L. Shang, N. R. Kelly, T. Anderson, and Z. K. Liu, "Thermodynamics of the S-Sn system: Implication for synthesis of earth abundant photovoltaic absorber materials," *Sol. Energy*, Vol. 125, pp. 314–323, 2016.
- [16] J. Camassel, M. Schlüter, S. Kohn, J. P. Voitchovsky, Y. R. Shen, and M. L. Cohen, "Wavelength Modulation Spectra and Electronic Band Structure of SnS₂ and SnSe₂," *Phys. Status Solidi*, Vol. 75, No. 1, pp. 303–314, 1976.
- [17] S. Nakashima, H. Katahama, and A. Mitsuishi, "The effect of polytypism on the vibrational properties of SnS₂," *Phys. B+C*, Vol. 105, No. 1–3, pp. 343–346, 1981.
- [18] Y. Huang, E. Sutter, J. T. Sadowski, M. Cotlet, O. L. A. Monti, D. A. Racke, M. R. Neupane, D. Wickramaratne, R. K. Lake, B. A. Parkinson, and P. Sutter, "Tin Disulfide; An Emerging Layered Metal Dichalcogenide Semiconductor: Materials Properties and Device Characteristics," No. 10, pp. 10743–10755, 2014.
- [19] A. K. Abass, H. A. Jassim, K. J. Majeid, and R. H. Misho, "Optical Parameters of Chemically Deposited Tin Disulfide," *Phys. Status Solidi*, Vol. 91, No. 1, pp. 129–133, 1985.
- [20] H. Zhong, G. Yang, H. Song, Q. Liao, H. Cui, P. Shen, and C. X. Wang, "Vertically aligned graphene-like SnS₂ ultrathin nanosheet arrays: Excellent energy storage, catalysis,

- photoconduction, and field-emitting performances,” *J. Phys. Chem. C*, Vol. 116, No. 16, pp. 9319–9326, 2012.
- [21] C. Shi, Z. Chen, G. Shi, R. Sun, X. Zhan, and X. Shen, “Influence of annealing on characteristics of tin disulfide thin films by vacuum thermal evaporation,” *Thin Solid Films*, Vol. 520, No. 15, pp. 4898–4901, 2012.
- [22] Y. Kumagai, L. A. Burton, A. Walsh, and F. Oba, “Electronic Structure and Defect Physics of Tin Sulfides: SnS, Sn₂S₃, and SnS₂,” *Phys. Rev. Appl.*, Vol. 6, No. 1, pp. 1–14, 2016.
- [23] N. G. Deshpande, A. A. Sagade, Y. G. Gudage, C. D. Lokhande, and R. Sharma, “Growth and characterization of tin disulfide (SnS₂) thin film deposited by successive ionic layer adsorption and reaction (SILAR) technique,” *J. Alloys Compd.*, Vol. 436, No. 1–2, pp. 421–426, 2007.
- [24] L. Amalraj, C. Sanjeeviraja, and M. Jayachandran, “Spray pyrolysed tin disulphide thin film and characterisation,” *J. Cryst. Growth*, Vol. 234, No. 4, pp. 683–689, 2002.
- [25] K. S. Kumar, C. Manoharan, L. Amalraj, S. Dhanapandian, G. Kiruthigaa, and K. Vijayakumar, “Spray deposition and characterization of undoped and In-doped tin disulphide thin films,” *Cryst. Res. Technol.*, Vol. 47, No. 7, pp. 771–779, 2012.
- [26] B. Thangaraju and P. Kaliannan, “Spray Pyrolytic Deposition and Characterization of SnS and SnS₂ Thin Films,” *J. Phys. D - Appl. Phys.*, Vol. 33, No. 9, pp. 1054–1059, 2000.
- [27] C. Khélia, K. Boubaker, T. Ben Nasrallah, M. Amlouk, and S. Belgacem, “Morphological and thermal properties of β-SnS₂ sprayed thin films using Boubaker polynomials expansion,” *J. Alloys Compd.*, Vol. 477, No. 1–2, pp. 461–467, 2009.
- [28] H. Search, C. Journals, A. Contact, M. Iopscience, and I. P. Address, “Effects of substrate temperature on absorption edge and photocurrent in evaporated amorphous SnS₂ films,” *J. Phys. D Appl. Phys.*, Vol. 136, No. 22, pp. 136–141, 1989.
- [29] S. Wang, S. Wang, J. Chen, P. Liu, M. Chen, H. Xiong, F. Guo, and M. Liu, “Influence of the deposition parameters on the properties of SnS₂ films prepared by PECVD method combined with solid sources,” *J. Nanoparticle Res.*, Vol. 16, No. 9, 2014.
- [30] S. K. Panda, A. Antonakos, E. Liarokapis, S. Bhattacharya, and S. Chaudhuri, “Optical properties of nanocrystalline SnS₂ thin films,” *Mater. Res. Bull.*, Vol. 42, No. 3, pp. 576–583, 2007.
- [31] K. T. R. Reddy, M. V. Reddy, M. Leach, J. K. Tan, D. Y. Jang, and R. W. Miles, “Crystalline behaviour of SnS layers produced by sulfurization of Sn films using H₂S,” *AIP Conf. Proc.*, Vol. 1447, No. 1, pp. 709–710, 2012.
- [32] A. S. Opanasyuk, D. I. Kurbatov, V. V. Kosyak, S. I. Kshniakina, and S. N. Danilchenko, “Characteristics of structure formation in zinc and cadmium chalcogenide films deposited on nonorienting substrates,” *Crystallogr. Reports*, Vol. 57, No. 7, pp. 927–933, 2012.
- [33] Y. P. Gnatenko, P. M. Bukivskij, A. S. Opanasyuk, D. I. Kurbatov, M. M. Kolesnyk, V. V. Kosyak, and H. Khlyap, “Low-temperature photoluminescence of II–VI films obtained by close-spaced vacuum sublimation,” *J. Lumin.*, Vol. 132, No. 11, pp. 2885–2888, Nov. 2012.
- [34] V. Kosyak, A. Opanasyuk, P. M. Bukivskij, and Y. P. Gnatenko, “Study of the structural and photoluminescence properties of CdTe polycrystalline films deposited by close-spaced vacuum sublimation,” *J. Cryst. Growth*, Vol. 312, No. 10, pp. 1726–1730, May 2010.
- [35] X. P. Zhan, C. W. Shi, X. J. Shen, M. Yao, and Y. R. Zhang, “Preparation of SnS Thin Films by Close-Spaced Sublimation at Different Source Temperatures,” *Adv. Mater. Res.*, Vol. 590, pp. 148–152, 2012.
- [36] M. G. Sousa, A. F. da Cunha, and P. A. Fernandes, “Annealing of RF-magnetron sputtered SnS₂ precursors as a new route for single phase SnS thin films,” *J. Alloys Compd.*, Vol. 592, pp. 80–85, Apr. 2014.
- [37] D. Avellaneda, B. Krishnan, T. K. Das Roy, G. A. Castillo, and S. Shaji, “Modification of structure, morphology and physical properties of tin sulfide thin films by pulsed laser irradiation,” *Appl. Phys. A*, Vol. 110, No. 3, pp. 667–672, Aug. 2012.
- [38] W. T. O. Bostanjoglo, F. E. Endruschat, “Time Resolved Tem of Laser-induced phase transitions in a-Ge and a-Si/Al-Films,” *Mater. Res. Soc.*, vol. 71, pp. 345–350, 1986.

- [39] W. Ettoumi, J. Kasparian, and J. P. Wolf, "Laser filamentation as a new phase transition universality class," *Phys. Rev. Lett.*, Vol. 114, No. 6, pp. 1–5, 2015.
- [40] E. Gatskevich, P. Příkryl, and G. Ivlev, "Modelling laser-induced phase transformations in semiconductors," *Math. Comput. Simul.*, Vol. 76, No. 1–3, pp. 65–72, 2007.
- [41] A. V. Ievlev, M. A. Susner, M. A. McGuire, P. Maksymovych, and S. V. Kalinin, "Quantitative Analysis of the Local Phase Transitions Induced by Laser Heating," No. 12, pp. 12442–12450, 2015.
- [42] N. Medvedev, H. O. Jeschke, and B. Ziaja, "Nonthermal phase transitions in semiconductors induced by a femtosecond extreme ultraviolet laser pulse," *New J. Phys.*, Vol. 15, 2013.
- [43] S. K. Sundaram and E. Mazur, "Inducing and probing non-thermal transitions in semiconductors using femtosecond laser pulses," *Nat. Mater.*, Vol. 1, No. 4, pp. 217–224, 2002.
- [44] X. C. Wang, H. Y. Zheng, C. W. Tan, F. Wang, H. Y. Yu, and K. L. Pey, "Femtosecond laser induced surface nanostructuring and simultaneous crystallization of amorphous thin silicon film," *Opt. Express*, Vol. 18, No. 18, p. 19379, 2010.
- [45] T. Cebriano, B. Méndez, and J. Piqueras, "Raman study of phase transitions induced by thermal annealing and laser irradiation in antimony oxide micro- and nanostructures," *CrystEngComm*, Vol. 18, No. 14, pp. 2541–2545, 2016.
- [46] A. Medvid, P. Onufrijevs, R. Jarimaviciute-Gudaitiene, E. Dauksta, and I. Prosycevas, "Formation mechanisms of nano and microcones by laser radiation on surfaces of Si, Ge, and SiGe crystals," *Nanoscale Res. Lett.*, Vol. 8, No. 1, p. 264, 2013.
- [47] A. Medvid, N. Litovchenko, A. Mychko, and Y. Naseka, "Exciton quantum confinement in nanocones formed on a surface of CdZnTe solid solution by laser radiation," *Nanoscale Res. Lett.*, Vol. 7, No. 1, p. 514, 2012.
- [48] A. Medvids, "Redistribution of Point Defects in the Crystalline Lattice of a Semiconductor in an Inhomogeneous Temperature Field," *Defect Diffus. Forum*, Vol. 210–212, pp. 89–102, 2002.
- [49] A. A. Voznyi, V. V. Kosyak, A. S. Opanasyuk, and V. M. Kuznetsov, "Structural Properties of the Sn_xS_y Films Obtained by the Thermal Vacuum Co-evaporation," *Proc. Int. Conf. Nanomater. Appl. Prop.*, Vol. 3, No. 1, pp. 1–4, 2014.
- [50] S. Prasert, "Development of Earth-Abundant Tin (II) Sulfide Thin-Film Solar Cells by Vapor Deposition," No. ii, p. 119, 2013.
- [51] L. Price, I. Parkin, A. Hardy, and R. Clark, "Atmospheric pressure chemical vapor deposition of tin sulfides (SnS, Sn₂S₃, and SnS₂) on glass," *Chem. Mater.*, No. 12, pp. 1792–1799, 1999.
- [52] V. G. Hadjiev, D. De, H. B. Peng, J. Manongdo, and A. M. Guloy, "Phonon probe of local strains in Sn_xSe_{2-x} mixed crystals," *Phys. Rev. B - Condens. Matter Mater. Phys.*, Vol. 87, No. 10, pp. 1–5, 2013.
- [53] H. R. Chandrasekhar, R. G. Humphreys, U. Zwick, and M. Cardona, "Infrared and Raman spectra of the IV-VI compounds SnS and SnSe," *Phys. Rev. B*, Vol. 15, No. 4, pp. 2177–2183, 1977.
- [54] H. Katahama, "Raman scattering study of interlayer bonding in CdI₂ AND SnS₂ under hydrostatic pressure: analysis by use of Van Der Waals interaction," *J. Phys. Chem. Solids*, Vol. 44, No. 11, pp. 1081–1087, 1983.
- [55] A. J. Smith, P. E. Meek, and W. Y. Liang, "Raman scattering studies of SnS₂ and SnSe₂," *J. Phys. Chem. C*, Vol. 1321, No. 10, p. 1321, 1977.
- [56] "Sn₂S₃ PDF-2 card No. 00-014-0619."
- [57] "SnS PDF-2 card No. 00-014-0620."
- [58] H. R. Chandrasekhar and D. G. Mead, "Long-wavelength phonons in mixed-valence semiconductor Sn II Sn IV S₃," *Phys. Rev. B*, Vol. 19, No. 2, pp. 932–937, Jan. 1979.
- [59] Q. Zai-Xiang, S. Yun, H. Wei-Yu, L. Wei, H. Qing, and L. Chang-Jian, "Raman scattering of polycrystalline GaSb thin films grown by the co-evaporation process," *Chinese Phys. B*, Vol. 18, No. 5, pp. 2012–2015, May 2009.